frontiers in Earth Science

ORIGINAL RESEARCH
published: 05 February 2019
doi: 10.3389/feart.2018.00249

Space-Based Imaging Radar Studies of U.S. Volcanoes

Daniel Dzurisin[1], Zhong Lu[2], Michael P. Poland[1] and Charles W. Wicks Jr.[3]*

[1] U.S. Geological Survey Cascades Volcano Observatory, Vancouver, WA, United States, [2] Roy M. Huffington Department of Earth Sciences, Southern Methodist University, Dallas, TX, United States, [3] United States Geological Survey, Menlo Park, CA, United States

The arrival of space-based imaging radar as a revolutionary land-surface mapping and monitoring tool little more than a quarter century ago enabled a spate of innovative volcano research worldwide. Soon after launch of European Space Agency's ERS-1 spacecraft in 1991, the U.S. Geological Survey began SAR and InSAR studies of volcanoes in the Aleutian and Cascades arcs, in Hawai'i, and elsewhere in the western U.S. including the Yellowstone and Long Valley calderas. This paper summarizes results of that effort and presents new findings concerning: (1) prevalence of volcano deformation in the Aleutian and Cascade arcs; (2) surface-change detection and hazard assessment during eruptions at Aleutian and Hawaiian volcanoes; (3) geodetic imaging of magma storage and transport systems in Hawai'i; and (4) deformation sources and processes at the Yellowstone and Long Valley calderas. Surface deformation caused by a variety of processes is common in arc settings and could easily escape detection without systematic InSAR surveillance. Space-based SAR imaging of active lava flows and domes in remote or heavily vegetated settings, including during periods of bad weather and darkness, extends land-based monitoring capabilities and improves hazards assessments. At Kīlauea Volcano, comprehensive SAR and InSAR observations identify multiple magma storage zones beneath the summit area and along the East Rift Zone, and illuminate magma transport pathways. The same approach at Yellowstone tracks the ascent of magmatic volatiles from a mid-crustal intrusion to shallow depth and relates that process to increased hydrothermal activity at the surface. Together with recent and planned launches of highly capable imaging-radar satellites, these findings support an optimistic outlook for near-real time surveillance of volcanoes at global scale in the coming decade.

Keywords: InSAR, Kīlauea, Three Sisters, Medicine Lake Volcano, Lassen volcanic center, Long Valley Caldera, Yellowstone Caldera, Aleutian volcanic arc

OPEN ACCESS

Edited by:
Federico Di Traglia,
Università degli Studi di Firenze, Italy

Reviewed by:
Andrea Bevilacqua,
University at Buffalo, United States
S. K. Ebmeier,
University of Leeds, United Kingdom

****Correspondence:***
Daniel Dzurisin
dzurisin@usgs.gov

Specialty section:
This article was submitted to Geohazards and Georisks, a section of the journal Frontiers in Earth Science

Received: *01 August 2018*
Accepted: *20 December 2018*
Published: *05 February 2019*

Citation:
Dzurisin D, Lu Z, Poland MP and Wicks CW Jr (2019) Space-Based Imaging Radar Studies of U.S. Volcanoes. Front. Earth Sci. 6:249. doi: 10.3389/feart.2018.00249

INTRODUCTION

The 1991 launch of European Space Agency's (ESA's) first European Remote Sensing satellite, ERS-1, afforded Earth scientists a powerful new tool for monitoring activity at the world's volcanoes. When traveling in the mission's primary mapping orbit, the C-band (wavelength λ = 5.66 cm) synthetic aperture radars (SARs) aboard ERS-1 and its companion, ERS-2 (launched in 1995) provided images of the entire globe at ~30 m spatial resolution across a swath width of 100 km with

an orbital repeat interval of 35 days. SAR's ability to image Earth's surface through meteorological clouds and in darkness immediately enabled surface-change detection and production of digital elevation models (DEMs) at many volcanoes that otherwise would not have been possible owing to remoteness or persistently poor weather.

Another quantum leap forward came with the realization that repeat-pass SAR images could be combined with a DEM to produce deformation interferograms, i.e., images depicting changes in slant range between the SAR and ground surface (essentially a snapshot of the surface deformation field) with centimeter-scale precision (Massonnet and Feigl, 1998). This revolutionary capability gained widespread attention when it was successfully applied to image deformation caused by the 1992 *M* 7.3 Landers earthquake (Massonnet et al., 1993). Almost overnight, a new field was born, satellite interferometric synthetic aperture radar (InSAR). Shortly thereafter, InSAR was used to map ground subsidence during and following the 1993 eruption of Mount Etna (Massonnet et al., 1995). Today, volcano scientists have access to centimeter-scale precision and high spatial resolution images of surface deformation over a wide area from InSAR, and to millimeter-scale precision and high temporal resolution data at selected locations from the Global Navigation Satellite System [GNSS, which includes the Global Positioning System (GPS)]. Combined with information from ground-based sensors, those capabilities enable detailed models of deformation sources (e.g., Segall, 2010) and three-dimensional mapping of magma storage and transport systems (e.g., Poland et al., 2014).

Space-based imaging radar systems provide two important capabilities with direct applications to volcano studies. The first is all-weather, 24/7 surface-change detection and imaging, which can be used to monitor volcanic processes such as lava flow inundation, lava dome growth, ash deposition, vent formation or enlargement, and surface faulting. Thus, SAR imagery can play an important role in assessing the potential for dome collapse and attendant pyroclastic density currents (e.g., Meyer et al., 2015; Wang et al., 2015).

A second capability of vital importance to volcano studies is geodetic imaging with InSAR. Numerous studies have used InSAR to map volcano deformation as a basis for inferring sources and processes, and to assess related hazards (e.g., Lu and Dzurisin, 2014, 2018; Pritchard and Yun, 2018; and references therein). In the United States, the first successful applications of InSAR to volcanoes were at the Katmai, Long Valley, and Yellowstone calderas (Lu, 1996; Lu et al., 1997; Thatcher and Massonnet, 1997; Wicks et al., 1998).

An outgrowth of those successes was a research project supported by the U.S. Geological Survey's (USGS) Volcano Hazards Program and its Volcano Science Center to apply SAR and InSAR capabilities to volcanoes in the U.S. and elsewhere. This paper reports project findings on: (1) prevalence of volcano deformation in the Aleutian and Cascade arcs; (2) surface-change detection and hazards assessment during eruptions at Aleutian and Hawaiian volcanoes; (3) geodetic imaging of magma storage and transport systems in Hawai'i; and (4) deformation sources and processes at the Yellowstone and Long Valley calderas. It serves as a snapshot of past and present USGS SAR/InSAR studies of volcanoes, with a look ahead to an expanded role for such studies in the next decade.

MATERIALS AND METHODS

For our research we used SAR data from various satellites operated by ESA (ERS-1/2, ENVISAT, Sentinel-1A/1B; C-band), Japan Aerospace Exploration Agency (JAXA) (JERS-1, ALOS-1/2; L-band), Canadian Space Agency (CSA) (RADARSAT-1; C-band), German Aerospace Center (DLR) (TerraSAR-X, TanDEM-X; X-band), and Italian Space Agency (ASI) (COSMO-SkyMed) (X-band). Additional information about each satellite system, including mission profiles and dates of operation, is tabulated in **Figure 2** by Elliott et al. (2016)[1]. To process the SAR data into interferograms, we used GAMMA software in conjunction with the highest resolution DEM available in each instance: ASTER Global Digital Elevation Map, Shuttle Radar Topography Mission (SRTM) DEM, USGS GMTED2010, or a custom DEM produced from SAR scenes.

GNSS data were processed by the USGS Earthquake Hazards Program using the GIPSY software package. Murray and Svarc (2017) provide a detailed description of the processing methodology.

To model the Yellowstone north-rim deformation sources (see below), we used available InSAR data from the ERS-2, ENVISAT, ALOS-2, Sentinel-1, TerraSAR-X, and RADARSAT-2 satellites. Acquisition dates for each scene are included in the caption for **Figure 6**. We also included GNSS data from stations in the USGS YellowstoneContin and Yellowstone_SPGPS networks[2]. Semipermanent GPS (SPGPS) is an alternative to continuous GPS and survey-mode GPS (also known as campaign-mode GPS) (Dzurisin et al., 2017). An SPGPS network consists of an array of threaded metal rods affixed to the ground that serve as benchmarks. Each rod is threaded so a GPS antenna can be mounted directly atop it, eliminating the need for a temporary tripod or a more permanent installation. The Yellowstone SPGPS network was established in 2008 and since has expanded to 12 stations; stations are deployed each year from about May through October when the surface is mostly snow-free. A non-linear inversion scheme with Monte Carlo starting models was used for all modeling. Additional details of the modeling strategy are provided as **Supplementary Material**.

RESULTS

Prevalence of Volcano Deformation in the Aleutian and Cascade Arcs

InSAR enables systematic surveillance of entire volcanic arcs, including the Aleutian and Cascade arcs; in both cases, our studies show that deformation is more prevalent than previously thought. Lu and Dzurisin (2014) examined each of 52 historically active volcanoes in the Aleutian arc

[1]https://www.nature.com/articles/ncomms13844

[2]https://earthquake.usgs.gov/monitoring/gps

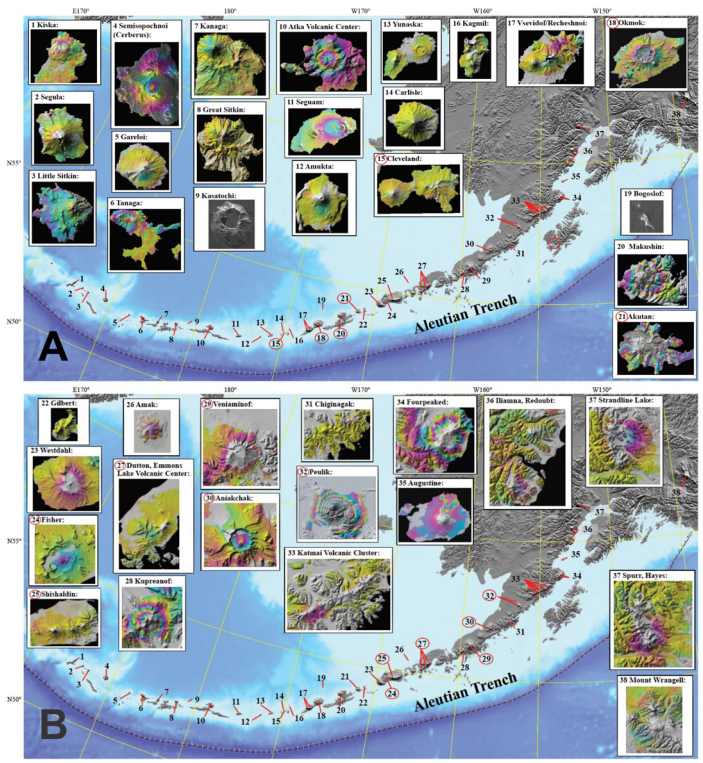

FIGURE 1 | Snapshots of InSAR-derived surface deformation at volcanoes in the western **(A)** and eastern **(B)** parts of the Aleutian arc. InSAR images span different intervals from the 1990s to 2010. All 52 historically active volcanoes were examined; only those with observed deformation are labeled. SAR images used come from ERS-1, JERS-1, ERS-2, Radarsat-1, Envisat, ALOS PALSAR-1, and TerraSAR-X. Number labels for volcanoes mentioned in the text are circled in red. For additional information, see Lu and Dzurisin (2014, 2018).

(**Figure 1**). Among the findings were: (1) volcano deformation is common and deformation styles are diverse, (2) many volcanoes deform without erupting, (3) deformation sources and associated eruptive vents are not always coincident; offsets can be up to several kilometers, (4) caldera systems are especially dynamic, and (5) space-based radar is a valuable tool for operational monitoring of surface change due to volcanic activity. Only 12 of the 52 volcanoes (23%) showed no evidence of surface deformation during the period of observation (1992–2010). Among those 12, Shishaldin (**Figure 1B**; #25) and Pavlof (**Figure 1B**, adjacent to Emmons Lake volcanic center, #27) erupted repeatedly without deforming, and deformation could have escaped detection at 8 others as a result of poor InSAR coherence or coverage. Therefore, deformation is the rule rather than exception at Aleutian volcanoes. Studies of other arcs and volcano-tectonic settings have produced similar results worldwide (e.g., Amelung et al., 2000; Pritchard and Simons, 2004a,b; Ebmeier et al., 2013), highlighting the importance of space-based radar as a tool for globally integrated volcano monitoring and research.

Volcano deformation in the Aleutian arc can have several causes, including magma intrusion or withdrawal, crystallization and volatile loss from magma, pressure changes in a hydrothermal system, and contraction of lava flows or pyroclastic deposits. Lu and Dzurisin (2014) concluded at least one episode of magma intrusion occurred beneath 21 of the 44 volcanoes (48%) for which useful InSAR observations were available. They observed shallow-seated subsidence at 11 of the 44 (25%), which they attributed to hydrothermal processes or contraction of surficial deposits. Three historically active caldera systems (Fisher, Emmons Lake, and Aniakchak) (**Figure 1B**; #24, #27, #30) exhibited deeper-seated subsidence attributed to cooling and volatile loss from crustal magma reservoirs. During the 18-year observation period, at least one eruption occurred at 17 of the 52 volcanoes examined (33%).

By comparison to other volcanic arcs that have been studied with InSAR or are well monitored by other means, these statistics demonstrate that the Aleutian arc is one of the most active on Earth. For example, Biggs et al. (2014) selected 198 volcanoes worldwide for which systematic InSAR observations are available throughout 1992–2010, the same period examined by Lu and Dzurisin (2014). They reported that 54 had deformed (27%) and 25 had erupted (13%) during the observation period. The corresponding percentages in the Aleutians were 77% (including all modes of deformation) and 33% (Lu and Dzurisin, 2014).

Lu and Dzurisin (2014) reported two somewhat contrariwise observations: (1) some Aleutian volcanoes erupt without deforming, and (2) others deform without erupting. Pritchard and Simons (2004a,b) reported similar behavior from their

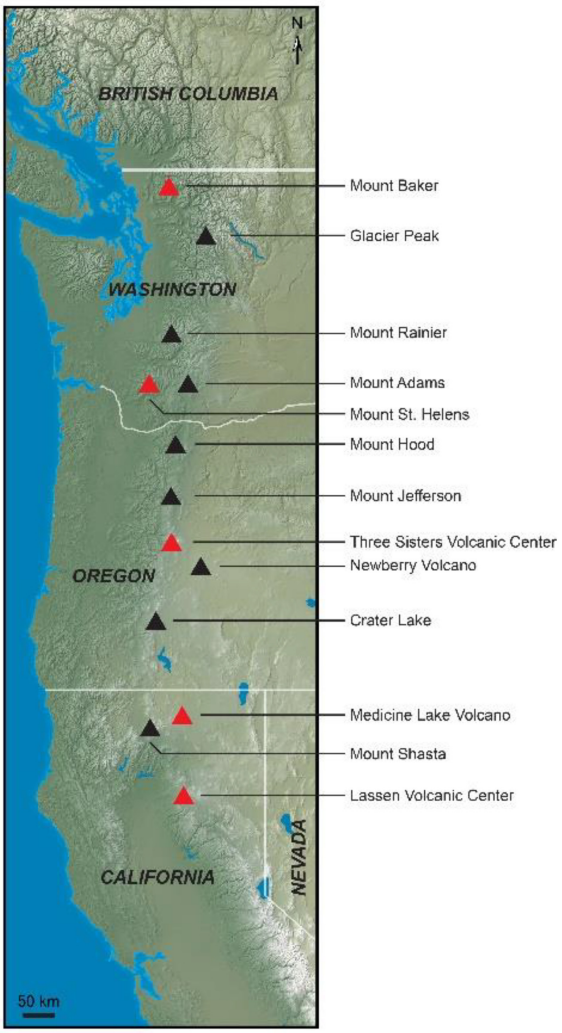

FIGURE 2 | Map of the major volcanic centers in the U.S. portion of the Cascade volcanic arc. Red colors indicate volcanoes where deformation has been detected. Modified from Poland et al. (2017).

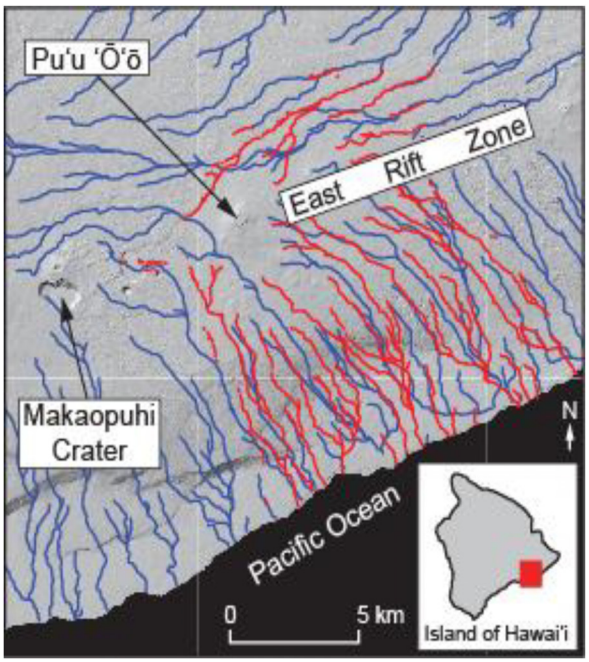

FIGURE 3 | Steepest descent lines indicating likely lava flow paths during the 1983–2018 Pu'u 'O'o-Kupaianaha eruption along Kīlauea's middle East Rift Zone. Blue lines show paths based on topographic data from 2005, whereas red lines are flow paths that were updated in 2013 using topographic information derived from bistatic TanDEM-X SAR imagery.

InSAR study of ∼900 volcanoes in the central Andes spanning 1992–2003. In the first category are mafic stratovolcanoes that erupt frequently. These are classified as open-conduit volcanoes, meaning that eruptions are frequent enough to maintain a hot and ductile conduit from a crustal magma reservoir to the near-surface. In the Aleutians, Cleveland, Shishaldin, and Pavlof (**Figures 1A,B**; #15, #25, #27) are prime examples. InSAR observations reveal no evidence of surface deformation at these volcanoes, even though they span at least two eruptions in each case. Greater magma flux through the lower crust along the central part of the arc, relative to the eastern and western segments, might be a factor in maintaining open conduits and producing frequent eruptions at these volcanoes.

Another observation from the InSAR survey of the Aleutian arc is that large caldera systems are especially dynamic. All 10 volcanic centers in the eastern Aleutian arc where one or more caldera-forming eruptions have occurred during Late Pleistocene or Holocene time (Miller and Smith, 1987), and with calderas larger than 3 km, deformed during 1992–2010. Four (Okmok, Makushin, Akutan, and Veniaminof) (**Figures 1A,B**; #18, #20, #21, #29) erupted at least once during that time and evidence of magma intrusion was identified at all four (Lu and Dzurisin, 2014). Three of the four (excluding Veniaminof) also experienced subsidence attributed to cooling and degassing of magma or hydrothermal systems, or to magma withdrawal.

Surface subsidence at various scales and rates is occurring at many Aleutian volcanoes and can be attributed to one of three causes. Where subsidence occurs on recent lava flows or pyroclastic flow deposits, the most likely cause is thermoelastic contraction as a result of cooling; surface loading by younger flows can also play a role (Lu et al., 2000a). In other cases, subsidence occurs in association with surface hydrothermal activity, with typical source depths 0–4 km below sea level. Such occurrences are attributed to depressurization by fluid loss (Lu and Dzurisin, 2014). A third type of subsidence, typically sourced 5–12 km below sea level, occurs in some areas that also experience uplift. This type is attributed to cooling and fluid loss from crustal magma reservoirs, because uplift and subsidence sources are essentially the same and some of the uplift episodes have culminated in eruptions (Lu and Dzurisin, 2014).

The study by Lu and Dzurisin (2014) also identified surface uplift attributed to magma intrusions at several volcanoes that have not erupted in more than a century. Examples are

Mount Recheshnoi (no reports of historical eruptions), Mount Kupreanof (no eruptions during Holocene time), and Mount Peulik (most recent eruption ∼160 years ago) (**Figure 1B**; #32). Such discoveries in the Aleutians and elsewhere (e.g., Three Sisters volcanic center in the Cascade arc; see below) demonstrate InSAR's utility for observing remote or sparsely monitored volcanoes, where unrest might otherwise go undetected.

The story is somewhat different in the Cascade arc (**Figure 2**), although InSAR has changed our thinking about the level of activity there as well. Prior to Mount St. Helen's reawakening in 1980, none of the Cascade volcanoes were known to be deforming. Since then, however, deformation has been detected at 5 of 13 (38%) major volcanic centers in the U.S. portion of the arc (Poland et al., 2017). InSAR was instrumental in the discovery of mostly aseismic, ongoing uplift at the Three Sisters volcanic center, discovery of subsidence at the Lassen volcanic center, and analysis of long-term subsidence at Medicine Lake Volcano; deformation at Mount St. Helens and Mount Baker is known from other techniques.

At Three Sisters, uplift of a broad area centered ∼5 km west of the summit of South Sister volcano was recognized in 2001 in ERS-1/2 interferograms that collectively span 1992–2000 (Wicks et al., 2002). Subsequent modeling of InSAR, leveling, and GPS observations indicates that uplift began in late 1997 or 1998, and the uplift rate declined steadily from a maximum of 3–5 cm/year during 1998–2001 to less than 0.5 cm/year when this was written in November 2018. Deformation was mostly aseismic, accompanied only by one swarm of ∼300 small earthquakes (M_{max} = 1.9) during March 23–26, 2004. The uplift episode is attributed to magma intrusion 5–7 km below the surface (Wicks et al., 2002; Dzurisin et al., 2005, 2009; Riddick and Schmidt, 2011). The most recent eruptions at South Sister produced rhyolitic tephra, pyroclastic flows, lava flows, and lava domes between 2.2 and 2.0 ka. Immediately north of Three Sisters, dominantly effusive eruptions of basaltic and andesitic lavas built large shield volcanoes and isolated cinder cones and lava flows as recently as 1.6 to 1.2 ka (Scott et al., 2001; Sherrod et al., 2004). It is not known how common intrusive events like the current one might have been in the interim.

Subsidence during 1996–2000 of a large area centered ∼5 km southeast of Lassen Peak in the Lassen volcanic center was discovered with InSAR and confirmed by comparing line lengths measured with EDM (1981, 1982, and 1984) and GPS (2004) (Poland et al., 2004). Parker et al. (2016) analyzed interferograms from ERS-1/2 (55 interferograms collectively spanning 1992–2000), ENVISAT (186, 2004–2010), and ALOS (16, 2007–2010) that revealed subsidence at an average rate of 10 mm/year from 1992 to 2010. They inferred a source depth of ∼8 km without expressing a preference among possible tectonic, magmatic, and hydrothermal mechanisms.

Long-term, steady subsidence of Medicine Lake Volcano at a maximum rate of 8.6 ± 0.9 mm/year was revealed by leveling surveys in 1954, 1989, and 1999 (Dzurisin et al., 1991, 2002). Poland et al. (2006) analyzed the leveling data together with GNSS and InSAR results and proposed a combination of gravitational loading by the volcanic edifice, tectonic extension, and cooling of magmatic intrusions as a likely cause of subsidence. Parker et al. (2014) showed that leveling, GNSS, and InSAR data were best fit with a deflating sill-like body at 9–10 km depth beneath the summit caldera, which they interpreted as consistent with the subsidence mechanisms proposed by Poland et al. (2006).

At Mount St. Helens, InSAR has identified a number of deformation sources that vary in time, space, and mechanism. Several isolated areas of the 1980 debris avalanche deposit are experiencing subsidence of ∼1–3 cm/year, possibly due to thermoelastic contraction of cooling deposits or compaction of poorly consolidated deposits (Poland and Lu, 2008). Co-eruptive deflation of the volcano was also detected during the first few months of the 2004–2008 eruption and attributed to pressure loss in a source more than 10 km beneath the edifice (Poland and Lu, 2008). Post-eruptive reinflation of the volcano (Dzurisin et al., 2015) was too small to be detected by InSAR, given the severe atmospheric artifacts that are common in interferograms of the volcano and that are difficult to mitigate (Foster et al., 2013), although subsidence of both the 1980–1986 and 2004–2008 lava domes (Poland et al., 2017) is apparent in high-resolution X-band interferograms of the volcano's crater.

Of 13 major volcanic centers in the Cascade Range (**Figure 2**), 10 are classified as Very High Threat, 2 as High Threat (Mount Adams, Medicine Lake Volcano), and 1 as Low Threat (Mount Jefferson) in the 2018 update to the USGS National Volcanic Threat Assessment (Ewert et al., 2018). The ranking is based on objective measures of volcano hazards and exposure of people and infrastructure to those hazards (Ewert et al., 2005; Ewert, 2007). Among the 12 Very High or High Threat volcanoes, 6 are located in wilderness areas where land management policies severely limit the number of monitoring stations (Mount Baker, Glacier Peak, Mount Adams, Three Sisters, Crater Lake, Mount Shasta). Especially at those volcanoes, InSAR is an essential monitoring tool to supplement sparse ground-based networks. Extensive snow cover precludes interferometric coherence during most of the year, but summer-to-summer interferograms are generally coherent except near the highest summits, where snow-cover persists year-round, and in heavily forested areas on some of the volcanoes' western flanks.

Prior to the advent of InSAR, conventional wisdom held that activity at most arc volcanoes could be characterized as long periods of dormancy punctuated by relatively brief eruptive episodes, with little or no detectable unrest in the interim. That view has changed with improvements in volcano monitoring techniques, including satellite imaging radar. Fully three-quarters of Aleutian volcanoes and one-third of Cascade volcanoes show evidence of ground deformation. In many cases deformation is not associated with eruptions, and in a few cases little or no other evidence of unrest is apparent.

Surface Change Detection and Hazard Assessment During Eruptions

Especially at remote or heavily vegetated volcanoes, surface change detection with SAR imagery complements other

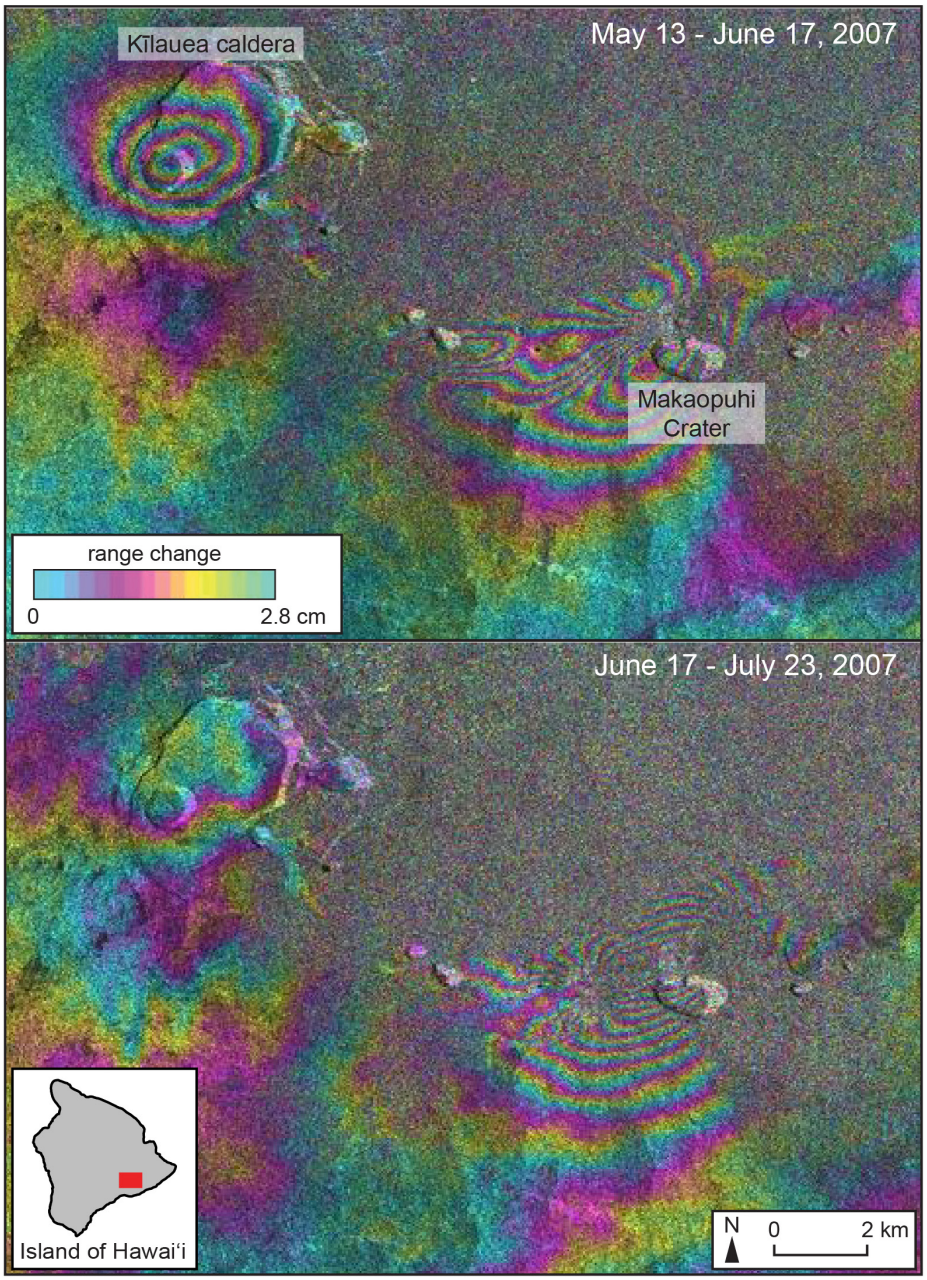

FIGURE 4 | ENVISAT interferograms from beam mode 2, track 93, and spanning the onset **(top)** and conclusion **(bottom)** of Kīlauea's July 17–19, 2007, East Rift Zone intrusion and eruption. This was one of the first times that a SAR image was acquired of a dike intrusion as it was happening, and the sequence of images provided excellent spatial resolution of how the intrusion evolved over time.

monitoring techniques and supports assessments of eruption impacts and hazards. For example, Meyer et al. (2015) described a system that integrates near real-time SAR data with a multidisciplinary volcano monitoring system developed at the Alaska Volcano Observatory and demonstrated its use to map both ground deformation and surface change by ash deposition during the 2008 eruption at Okmok volcano (**Figure 1A**; #18). Wang et al. (2015) used time-sequential TerraSAR-X SAR images to track eruptive activity at Mount Cleveland volcano (**Figure 1A**; #15), where visual observations were hampered by persistent bad weather and the volcano's remote location in the central Aleutian arc. They were able to document growth of a lava dome and confirm that any eruption-related deformation did not extend beyond the ∼200-m diameter summit crater where the dome grew. Surface scattering characteristics changed rapidly during extrusion, preventing retrieval of reliable phase change or pixel offset information from SAR images. Instead, Wang et al. (2015) used feature tracking of bright scatterers

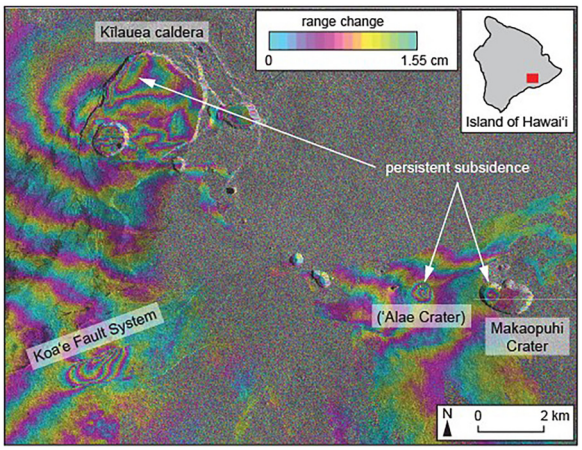

FIGURE 5 | Cosmo-SkyMed interferogram spanning April 2, 2012 – March 19, 2014 and showing deformation of Kīlauea's summit area and upper/middle East Rift Zone. Isolated areas of subsidence in the East Rift Zone at 'Alae and Makaopuhi Craters are due to cooling of lava that filled those craters during the 1969–1974 Mauna Ulu eruption. A similar origin is expected for subsidence in the north part of Kīlauea caldera, where a lava lake existed in the 1800s. Localized fringes in the Koa'e fault system are due to a pair of ~M 3.5 earthquakes on June 4–5, 2012.

together with knowledge of the SAR imaging geometry and a dome growth simulation to calculate the height and area of the dome as a function of time, and thus to estimate the extrusion rate. Results indicate the dome grew at rates as high as 0.6 m^3/s to a maximum height of nearly 70 m with a basal area of 0.025 km^2. No coeruptive surface deformation was detected beyond the crater rim, consistent with the inference of Lu and Dzurisin (2014) that most eruptions at Cleveland are fed from a persistently open conduit without disturbing the surrounding edifice.

Akutan volcano (**Figure 1A**; #21) is similar to Cleveland in that both are in the central part of the arc and both erupt frequently—Akutan 16 times from 1962 to 1992—but they differ markedly in one respect. In March 1996, more than 200 earthquakes larger than magnitude 3.5 occurred at Akutan, accompanied by a complex deformation pattern with ~60 cm of uplift and a zone of ground cracks up to 500 meters wide and more than 3 km long. Modeling of InSAR observations suggests these were manifestations of dike intrusion to within a few hundred meters of the surface, although no eruption ensued (Lu et al., 2000b, 2005a,b). Recent InSAR and GNSS observations confirm that steady inflation at Akutan was punctuated by intrusions accompanied by seismic swarms in 2008 and 2014, although activity was less intense in those cases than during the 1996 episode (Degrandpre et al., 2017; Wang et al., 2018). Differences in behavior at Cleveland and Akutan (the first typically erupts without deforming, the second sometimes deforms without erupting) presumably reflect differences in local tectonic setting or crustal structure that facilitate an open/ductile magma conduit at Cleveland (also Shishaldin and Pavlof, with similar behavior), but not at Akutan.

In Hawai'i, SAR has contributed to monitoring surface inundation by lava flows and to forecasting flow paths in support of hazards assessments. SAR surveillance at Kīlauea began in 1984 with Shuttle Imaging Radar (SIR-B) data, which Gaddis et al. (1989) demonstrated could be useful for distinguishing surface characteristics (e.g., lava flow versus pyroclastic deposit). Zebker et al. (1996) demonstrated SAR's potential for mapping lava flows based on changes in interferometric coherence in SIR-C images over time. Building on Zebker et al.'s (1996) approach, Dietterich et al. (2012) showed that coherence imagery from multiple look angles could be combined to produce a map of lava flow emplacement with temporal resolution on the order of days. This is far more frequent than ground- or air-based data are collected by the USGS Hawaiian Volcano Observatory (HVO) (except during a crisis) and has the benefit of seeing through weather clouds that might block other remote means of lava flow mapping (e.g., satellite thermal imaging).

In another application, InSAR can be used to update topographic maps in areas of active lava flows. Poland (2014) exploited bistatic TanDEM-X data to create sequential DEMs of an active flow field and calculate lava discharge rate from Kīlauea's East Rift Zone during 2012. This information, which would not otherwise be known, helped constrain temporal variability in magma supply to Kīlauea (Anderson and Poland, 2016). The new topography also was used to update models used by the Hawaiian Volcano Observatory to forecast lava flow pathways. These models, which are based on topographic steepest-descent calculations (Kauahikaua et al., 2003; Kauahikaua, 2007), are only accurate until new flows are emplaced, which alters the topography. InSAR provides a means of updating the topographic information, allowing for the generation of updated flow-path models—a critical capability during any ongoing eruption. For example, in 2013, lava flows from the East Rift Zone eruptive vent at Kīlauea Volcano, Hawai'i, stopped flowing southeast toward the sea, and instead accumulated around the vent and eventually flowed to the northeast (Patrick et al., 2015), precipitating a lava flow crisis in the village of Pāhoa (Poland et al., 2016). When lava flow activity returned to the coastal area in 2016, the Hawaiian Volcano Observatory used topographic information that was updated from TanDEM-X SAR data collected in 2013 to recalculate the steepest descent pathways, which had been based on topographic data from 2005 (**Figure 3**). The updated topography informed forecasts of lava flow paths that were communicated by the Hawaiian Volcano Observatory to local emergency managers.

Geodetic Imaging of Magma Storage and Transport Systems at Kīlauea and Mauna Loa

Hawaiian volcanoes are among the best monitored in the world, especially in terms of ground deformation. A variety of volcano-monitoring techniques have been developed and tested there, including both classical methods, like single-setup leveling and electronic distance measurement (EDM, Decker et al., 2008), and modern tools like SAR and InSAR. Some of the first InSAR deformation maps of an active volcano

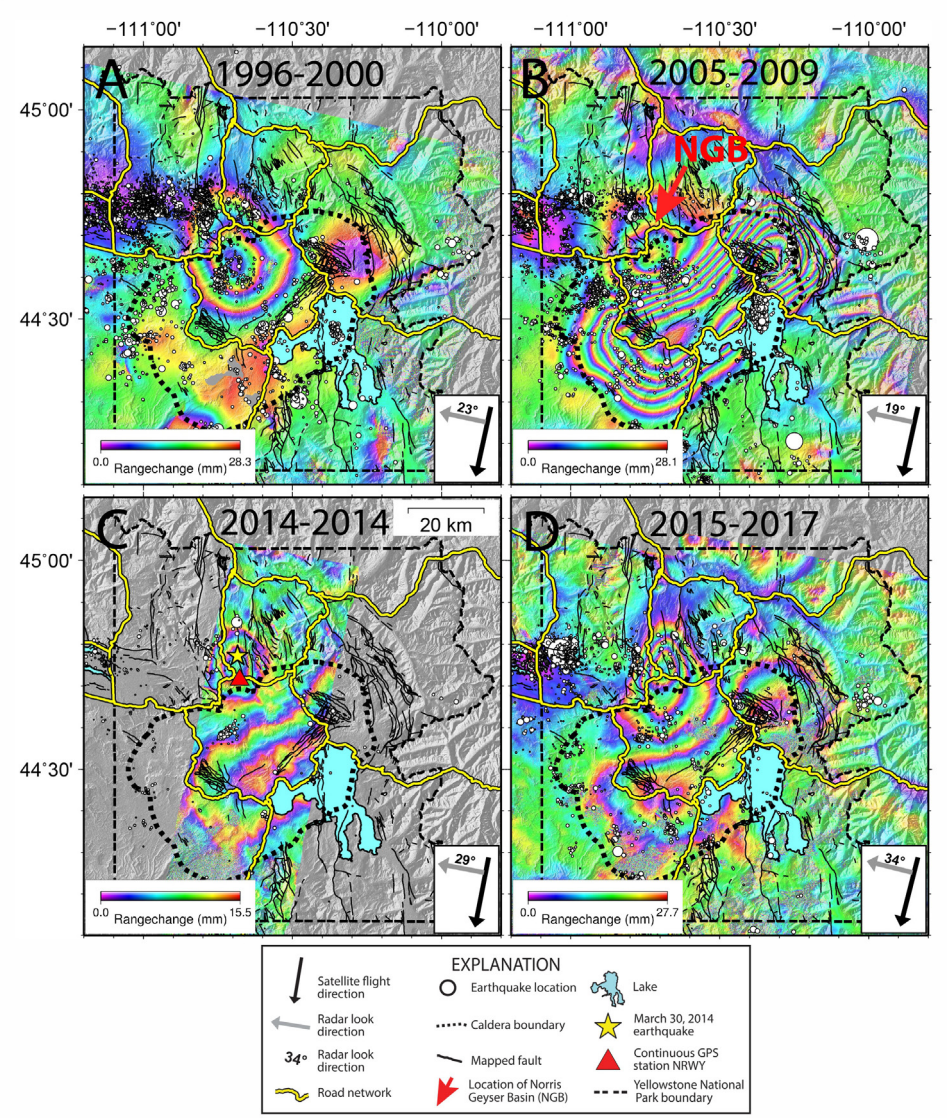

FIGURE 6 | Four interferograms representing evolution of north-rim deformation sources since 1996. Period in years spanned by each interferogram is labeled near top of each panel. Color bar showing range change mapping in each interferogram is in lower left corner of each panel and radar geometry is shown in lower right corner of each panel. Caldera boundary, Yellowstone National Park Boundary, and mapped faults are from Christiansen (2001). Earthquake circle size is scaled to magnitude. **(A)** ERS-2 interferogram from 19960919 to 20000928. **(B)** ENVISAT interferogram from 20050802 to 20090811. **(C)** TerraSARX interferogram from 20140609 to 20141008. The 20 km length scale in upper right of panel C applies to all panels. **(D)** Sentinel 1 interferogram from 20150727 to 20171020.

were SIR-C interferograms spanning days to months in 1994 (Rosen et al., 1996). However, lack of a ground-based receiving station for much of the 1990s limited SAR data acquisition for Hawai'i, since the ERS-1/2 satellites did not have on-board recorders. Therefore, application of SAR/InSAR to Hawaiian volcanoes was sparse prior to the availability of data from RADARSAT-1 in 1997 and ENVISAT in 2003. These datasets were the first in an explosion of SAR imagery that was enhanced in 2008 by the establishment of Hawaiian Volcanoes as the first Geohazards Supersite of the Geohazards Supersites and Natural Laboratories (GSNL) initiative of the Group on Earth Observations.

Geohazards Supersites were developed to encourage scientific exploration of earthquake and volcano hazards for the purpose of improving disaster risk management (Salvi et al., 2017). Hawaiian Volcanoes is one of ten permanent Supersites distributed around the globe. The Supersite charter and a list of permanent Supersites are at https://geo-gsnl.org/supersites/permanent-supersites/. Among other functions, Supersites provide open access to satellite and ground-based geophysical datasets from different sources and different disciplines (e.g., seismic, GNSS, volcanic gas, gravity, LIDAR).

With Hawai'i as a Geohazards Supersite, imagery from numerous SAR satellites, as well as ground-based data (like

seismic and geodetic measurements collected by HVO), are freely available to the scientific community. Studies based on these datasets have benefited not only research into Hawaiian volcanism, but also the development of new methods for integrating SAR and ground-based data and extracting the maximum possible signal from interferograms, especially in the along-track direction of SAR satellites (e.g., Chen et al., 2014; Jo et al., 2015). Some SAR datasets are provided to the Supersite with a latency of only hours, which facilitates the timely use of interferometric data in monitoring and hazards assessment.

InSAR results in Hawai'i have provided a wealth of information about the magmatic systems of Kīlauea and Mauna Loa volcanoes. The spatial detail provided by interferograms has been especially important for mapping the spatial and temporal complexity of summit magma storage at Mauna Loa (e.g., Amelung et al., 2007) and Kīlauea (e.g., Baker and Amelung, 2012; Poland et al., 2014). In addition, InSAR has been invaluable for supplying important observations of known processes, especially magmatic intrusions. For example, Kīlauea's 1993 East Rift Zone intrusion was known from tilt and seismicity, but JERS interferograms provided otherwise unavailable constraints on the volume of the intrusion (Conway et al., 2018). Even in the presence of robust continuous tilt and GPS networks that were installed in the late 1990s, interferograms still offered much needed constraints on models of dike emplacement, like that of the 1999 Kīlauea East Rift Zone intrusion (Cervelli et al., 2002). A leap forward was achieved in 2007, when SAR data were acquired in the middle of a dike emplacement event (**Figure 4**). The serendipitous timing allowed for detailed modeling of the temporal evolution of the intrusion, especially when combined with tilt and GNSS data (Montgomery-Brown et al., 2010, 2011). A 2011 East Rift Zone fissure eruption was imaged in even greater temporal detail, with multiple SAR satellites acquiring data before, during, and after the 4.5-day-long event. These data were especially valuable because the eruption occurred in an area of sparse geodetic stations, and they enabled modeling of the intrusion's volume over time (Lundgren et al., 2013).

Less appreciated is the role of InSAR in discovering small-scale features that would not otherwise be known, given the poor spatial resolution of ground-based sensors. For example, interferograms of Kīlauea reveal relatively small, persistent subsidence features at the summit and along the volcano's East Rift Zone (**Figure 5**). The summit feature is located within the northern part of the summit caldera in an area of a former lava lake from the 1800s and might represent cooling of a thick lava pile, even though those flows are well over 100 years old. The East Rift Zone subsidence features coincide with the locations of former pit craters—'Alae Crater and a deep part of Makaopuhi Crater—that were filled by lava during the 1969–1974 Mauna Ulu eruption. Cooling and contraction of these thick accumulations of lava is clearly driving subsidence at these locations. Interferograms have also been instrumental in identifying areas prone to collapse, for example, along the rim of the summit eruptive vent that opened in 2008 (Richter et al., 2013) and on supposedly stable land near the lava-ocean entry (Poland and Orr, 2014). InSAR has even been important for detecting subtle features associated with earthquakes, from small (∼M 3) shallow seismic events in the Koa'e Fault System between Kīlauea's summit caldera and the coast (Swanson et al., 2018) (**Figure 5**), to isolated areas of subsidence on the western side of the island (mostly in Mauna Loa lava flows) that were associated with a magnitude M 6.7 earthquake in 2006 and are thought to be a result of surface settling due to strong shaking (Poland, 2010).

A large effusive eruption along Kīlauea's lower East Rift Zone and major collapse of the summit area was initiated by the onset of a dike intrusion on 30 April 2018 and was accompanied by a magnitude 6.9 earthquake beneath the volcano's south flank on 4 May. The first of many small explosions from the summit occurred on 16 May; resulting ash plumes reached as high as ∼3 km above sea level. Lava effusion and summit collapse stopped in early August 2018. SAR and InSAR observations played a vital role in tracking both summit collapse and lava inundation paths during the 2018 activity. Interferograms provided timely (every 1–3 days) and spatially broad coverage of volcano-wide deformation, including both rift zone spreading and summit subsidence. Amplitude images were also valuable in constraining the changing geometry of lava flows on the lower East Rift Zone, as well as tracking the development of faults and collapse structures at the summit over time (despite weather that occasionally obscured visual observations). SAR data, provided within hours of acquisition by some agencies thanks in part to Hawai'i's status as a GSNL Supersite, provided an operational awareness of deformation and surface change during the crisis that was critical to informing assessments of activity and forecasts of potential future changes. For example, the lack of continued spreading of the lower East Rift Zone after the first few weeks of the eruption suggested a low probability of farther downrift dike propagation, and spatial patterns of summit subsidence indicated that volume loss was mostly occurring from the shallower and smaller of two primary subsurface magma storage areas in the summit area.

Deformation Sources and Processes at the Yellowstone and Long Valley Calderas

High spatial resolution InSAR observations, especially when combined with high temporal resolution GNSS observations, can be inverted to produce source models of sufficient detail to effectively image entire magma storage and transport systems. At Yellowstone, repeated leveling surveys had revealed years-to-decades long episodes of surface uplift and subsidence of the caldera floor (Dzurisin et al., 2012) when an adjacent deformation center along the north caldera rim near Norris Geyser Basin (one of the hottest thermal areas within the Yellowstone magmatic system) was identified with campaign-mode GNSS and InSAR observations (Wicks et al., 1998; Meertens et al., 2000) (**Figures 6A,B**). In the succeeding two decades, the Norris area has been especially dynamic, with rapid uplift episodes interspersed with periods of subsidence. Inside the caldera, InSAR has been used to map surface deformation in greater spatial detail than is possible with leveling or GNSS, thereby strengthening observational constraints on source models (Wicks et al., 1998, 2006; Chang et al., 2007, 2010).

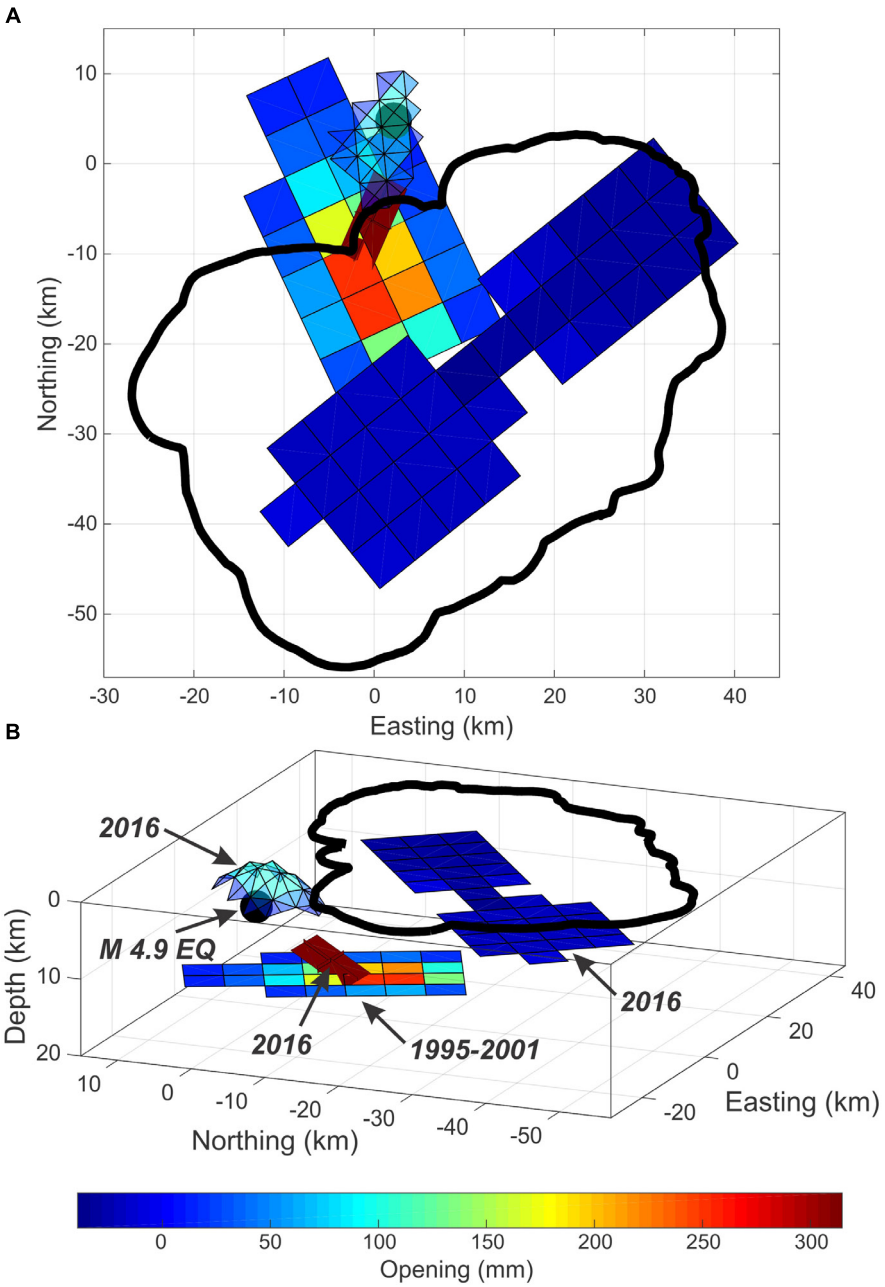

FIGURE 7 | Source models for deformation events discussed in the text. Flat-lying source under north caldera rim is for 1995–2001 uplift episode there. All other sources are for deformation that occurred during 2016, including domed and tabular expansion sources under the north caldera rim and a sill-like contraction source under the caldera floor. Black sphere shows location of March 30, 2014, M 4.9 earthquake (see **Figure 6C**). Color bar at bottom shows millimeters of opening. **(A)** Plan view of sources. **(B)** Perspective view of sources from WSW.

InSAR was essential in following a north-rim deformation episode that began as uplift in 1995, progressed through 2001 when it essentially ceased, then switched to subsidence in 2004 (**Figures 6A,B**). Uplift at a rate of 20–30 cm/yr resumed in late 2013, but abruptly reversed to subsidence following a Mw 4.9 earthquake on March 30, 2014 (**Figure 6C**). Subsidence stopped in early 2015 but was followed by another uplift episode that began in early 2016 (**Figure 6D**) and was continuing when this was written in November 2018. By that date, uplift measured at continuous GNSS station NRWY, about 5 km SSE of the center of uplift identified with InSAR, had reached nearly 10 cm, while central parts of the caldera floor had subsided 1–4 cm.

Figure 7 shows best-fit sources for the 1995–2001 north-rim uplift episode and for deformation from early 2016 to present for both the north rim (uplift) and caldera floor (subsidence). The source for the 1995–2001 north-rim episode is a distribution

of Okada (1985) dislocation sources that follow a 2-D Weibull distribution (Myrhaug and Rue, 1998), centered about 14 km below the surface. The early 2016 to present source beneath the caldera consists of two separate 2-D Weibull distributions confined to the same plane at a depth of 5–8 km. The same source also fits the caldera-floor deformation from late 2013 to early 2014. The source for the early 2016 to present north-rim uplift episode comprises two parts: (1) a shallow domed source of triangular dislocations (Nikkhoo and Walter, 2015) in which the depth variation of the reservoir follows one 2-D Weibull distribution and the amount of opening follows another, and (2) a deeper compound dislocation source (Nikkhoo et al., 2017). The source for the late 2013 to early 2014 north-rim uplift episode (not shown in **Figure 6**) is similar to the shallow domed source for the early 2016 to present episode, except the latter is somewhat shallower: about 3 km below the surface to the shallowest part of the 2013–2014 source, and about 2 km below the surface for the 2016–present source.

We suggest that north-rim uplift during 1995–2001 was caused by a magmatic intrusion at about 14 km depth beneath Norris Geyser Basin. The two more recent uplift episodes there might indicate upward migration and accumulation of volatiles exsolved from the earlier intrusion, perhaps along a pathway represented by the dipping tabular body shown in **Figure 7**. The process was rapid in late 2013 and early 2014, leading to the March 30, 2014, Mw 4.9 earthquake. Fracture permeability created by the earthquake might account for the temporary reversal to north-rim subsidence, and self-sealing by mineral deposition or quasi-plastic flow (Fournier, 1999, 2007) might explain the resumption of uplift in early 2016. Shallowing of the north-rim deformation source from ∼3 km depth in 2014 to ∼2 km depth in 2016 suggests that upward migration of volatiles is continuing. Any connection between north-rim uplift sources and caldera-floor subsidence sources during the study period was not revealed by our modeling. Steamboat Geyser, the highest geyser in the world, is situated in Norris Geyser Basin and often goes many years between eruptions. When this was written in November 2018, Steamboat had erupted 25 times since March 15, 2018. The frequent eruptions might be the result of surface dilatation from the ongoing uplift episode or an influx of magmatic heat and volatiles from the 1995–2001 intrusion.

InSAR measurements also have played an important role at Long Valley Caldera, which has experienced several episodes of surface uplift since 1980 (Savage and Clark, 1982; Castle et al., 1984; Hill, 1984; Savage, 1988; Langbein, 1989; Thatcher and Massonnet, 1997; Langbein, 2003). Two deformation sources have been identified, one beneath the resurgent dome at 6–7 km depth and another beneath the caldera's south moat at 10–20 km depth. Langbein (2003) attributed both sources to magmatic inflation, in the south moat accompanied by right-lateral fault motion.

The most recent uplift episode began in 2011, coincident with renewed swarm seismicity. Montgomery-Brown et al. (2015) analyzed the deformation using a combination of GPS and TerraSAR-X InSAR data, the latter processed using a persistent scatterer technique. They showed that the data are well fit by an inflation source ∼7 km beneath the resurgent dome, consistent with results for previous inflation episodes. A second source beneath the south most is permissible but not well resolved by the data.

Similar to Yellowstone in size and age, Long Valley differs in that only minimal subsidence has occurred between uplift episodes there (Tizzani et al., 2009; Liu et al., 2011; Montgomery-Brown et al., 2015), whereas at Yellowstone subsidence has been nearly as prevalent and pronounced as uplift (Dzurisin et al., 2012). Montgomery-Brown et al. (2015) suggested the difference might indicate that episodic discharge of hydrothermal fluids, which Waite and Smith (2002) proposed as a mechanism for caldera subsidence at Yellowstone, might be less important at Long Valley.

Although our interpretation of source models for 1995-to-present deformation along the north rim of Yellowstone Caldera is speculative, it supports a plausible narrative based on decades of multidisciplinary research there. Intrusions of basaltic magma in the mid- to lower crust are required to sustain the very high surface fluxes of heat and CO_2 (Werner and Brantley, 2003; Lowenstern and Hurwitz, 2008), large $^3He/^4He$ ratios indicate a dominantly magmatic source for fumarolic gases (Craig et al., 1978), and volatile accumulation/release in the upper crust has been proposed as a mechanism for uplift/subsidence cycles (Fournier, 1999, 2007). For the first time, modeling of high-spatial-resolution InSAR observations of the north rim area resolves multiple deformation sources in the mid- to upper crust that can be interpreted as evidence of magma intrusion followed by volatile exsolution, migration, accumulation, and escape. By extension, similar processes might be occurring at Long Valley, although the relative absence of subsidence there points to a lesser role for escape of magmatic volatiles to the surface.

DISCUSSION

Based on the wealth of new information about volcanic systems and processes garnered in recent decades, we can expect space-based imaging radar to remain an effective volcano monitoring and research tool for the foreseeable future. Recent and planned launches of SAR satellites will enable hourly-to-daily monitoring of many volcanoes worldwide at different wavelengths and from multiple viewing geometries (Elliott et al., 2016), providing more timely monitoring of surface change and tighter constraints on deformation models. For example, Finland's ICEYE project plans a constellation of more than 18 SAR microsatellites to provide high-resolution imaging of the entire globe every few hours—a capability with obvious applications to change detection at volcanoes. ICEYE-X1 was launched successfully in January 2018. Spain's first SAR satellite, PAZ, was launched in February 2018 and forms a constellation with Germany's TerraSAR-X and TanDEM-X satellites. The first TerraSAR-X NG (Next Generation) satellite is scheduled for launch in 2018–2019, and Italy's second-generation COSMO-SkyMed satellites (CSG 1, 2) in 2018–2020. At C-band, the three-satellite RADARSAT Constellation Mission (RCM) is scheduled to start in 2018–2019. NISAR, a joint United States-India SAR mission focused on natural processes and hazards, is expected to launch in 2020 with

both L-band and S-band polarimetric SARs abroad. A torrent of volcano SAR data will arrive soon and continue years into the future.

As new satellites become operational, multi-temporal InSAR observations will continue to be combined with deformation data from GNSS networks, *in situ* sensors including tiltmeters and strainmeters, and from other disciplines including seismology and geochemistry to develop and refine volcano models. Advances in computing capability and data processing techniques will enable routine, timely production of SAR and InSAR images for most of Earth's land surface area, to the extent that space-based radar observations will become a readily accessible data stream for volcanologists worldwide, and a staple of global volcano monitoring efforts. In the U.S., space-based radar will continue to play an essential role in monitoring activity along the Aleutian and Cascade volcanic arcs, in studying all aspects of basaltic volcanism in Hawai'i, and in tracking deformation episodes at Yellowstone and Long Valley calderas. Physics-based models eventually may lead to more accurate forecasts of activity at Mount St. Helens, Kīlauea, and Mauna Loa, and help to identify mechanisms of unrest at large silicic magma systems including Yellowstone and Long Valley.

InSAR is likely to contribute to improved eruption and hazards forecasts in two ways. First, its high spatial resolution and shorter repeat times made possible by planned launches of additional SAR satellites will enable tighter constraints on the locations, shapes, and physical interpretations of deformation sources, which in turn serve as starting points for physics-based models that forecast eruptive activity in a probabilistic framework (e.g., Anderson and Segall, 2013). Second, more frequent SAR observations will enable more detailed tracking of dome growth and lava-flow inundation at remote volcanoes – information that supports improved hazards forecasts. Regarding mechanisms of caldera unrest, the work reported here concerning activity at Yellowstone since 1995 is a first step toward integrating deformation source models that evolve over time with magmatic processes that do the same, e.g., magma intrusion, volatile exsolution and ascent, and surficial hydrothermal activity. InSAR's high spatial resolution was essential for recognizing subtle differences in the 2013–2014 and 2016–present deformation fields, which informed our interpretation of upward migration of trapped volatiles and a possible link to increased activity at Steamboat Geyser.

AUTHOR CONTRIBUTIONS

DD took the lead in compiling the manuscript and responding to reviews. ZL contributed the Aleutians section. MP contributed the Hawai'i section. CW contributed the Yellowstone section.

FUNDING

This research was supported in part by the U.S. Geological Survey's Volcano Hazards Program and Volcano Science Center through the InSAR Applied to Volcano Studies project at the USGS Cascades Volcano Observatory. ZL was supported by the National Aeronautics and Space Administration's (NASA) Earth Surface and Interior Program (NNX14AQ95G), NASA Geodetic Imaging Program (NNX16AK56G), and the Shuler–Foscue Endowment at Southern Methodist University. Any use of trade, firm, or product names is for descriptive purposes only and does not imply endorsement by the U.S. government.

SUPPLEMENTARY MATERIAL

The Supplementary Material for this article can be found online at: https://www.frontiersin.org/articles/10.3389/feart.2018.00249/full#supplementary-material

REFERENCES

Amelung, F., Jónsson, S., Zebker, H., and Segall, P. (2000). Widespread uplift and 'trapdoor' faulting on Galápagos volcanoes observed with radar interferometry. *Nature* 407, 993–996. doi: 10.1038/35039604

Amelung, F., Yun, S.-H., Walter, T. R., Segall, P., and Kim, S.-W. (2007). Stress control of deep rift intrusion at Mauna Loa Volcano, Hawai'i. *Science* 316, 1026–1030. doi: 10.1126/science.1140035

Anderson, K., and Segall, P. (2013). Bayesian inversion of data from effusive volcanic eruptions using physics-based models: application to Mount St. Helens 2004–2008. *J. Geophys. Res. Solid Earth* 118, 2017–2037. doi: 10.1002/jgrb.50169

Baker, S., and Amelung, F. (2012). Top-down inflation and deflation at the summit of Kīlauea Volcano, Hawai'i observed with InSAR. *J. Geophys. Res.* 117:14. doi: 10.1029/2011JB009123

Anderson, K. R., and Poland, M. P. (2016). Bayesian estimation of magma supply, storage, and eruption rates using a multiphysical volcano model; Kīlauea Volcano, 2000–2012. *Earth Planet. Sci. Lett.* 447, 161–171. doi: 10.1016/j.epsl.2016.04.029

Biggs, J., Ebmeier, S. K., Aspinall, W. P., Lu, Z., Pritchard, M. E., Sparks, R. S. J., et al. (2014). Global link between deformation and volcanic eruption quantified by satellite imagery. *Nat. Commun.* 5:3471. doi: 10.1038/ncomms4471

Castle, R. O., Estrem, J. E., and Savage, J. C. (1984). Uplift across long Valley caldera, California. *J. Geophys. Res.* 89, 11507–11516. doi: 10.1029/JB089iB13p11507

Cervelli, P., Segall, P., Amelung, F., Garbeil, H., Owen, S., Miklius, A., et al. (2002). The 12 September 1999 upper east rift zone dike intrusion at Kīlauea Volcano, Hawai'i. *J. Geophys. Res.* 107:13. doi: 10.1029/2001JB000602

Chang, W. L., Smith, R. B., Farrell, J., and Puskas, C. M. (2010). An extraordinary episode of Yellowstone caldera uplift, 2004–2010, from GPS and InSAR observations. *Geophys. Res. Lett.* 37:L23302. doi: 10.1029/2010GL045451

Chang, W. L., Smith, R. B., Wicks, C., Farrell, J., and Puskas, C. M. (2007). Accelerated uplift and magmatic intrusion of the Yellowstone caldera, 2004 to 2006. *Science* 318, 952–956. doi: 10.1126/science.1146842

Chen, J., Zebker, H. A., Segall, P., and Miklius, A. (2014). The 2010 slow slip event and secular motion at Kīlauea, Hawai'i inferred from TerraSAR-X InSAR data. *J. Geophys. Res.* 119, 6667–6683. doi: 10.1002/2014JB011156

Christiansen, R. L. (2001). *The Quaternary and Pliocene Yellowstone Plateau Volcanic Field of Wyoming, Idaho, and Montana*. Reston, VA: U.S. Geological Survey, 120. Available at: https://pubs.usgs.gov/pp/pp729g

Conway, S., Wauthier, C., Fukushima, Y., and Poland, M. (2018). A retrospective look at the February 1993 East Rift Zone intrusion at Kīlauea volcano, Hawai'i. *J. Volcanol. Geotherm. Res.* 358, 241–251. doi: 10.1016/j.jvolgeores.2018.05.017

Craig, H., Lupton, J. E., Welhan, J. A., and Poreda, R. (1978). Helium isotope ratios in Yellowstone and Lassen Park volcanic gases. *Geophys. Res. Lett.* 5, 897–900. doi: 10.1029/GL005i011p00897

Decker, R., Okamura, A., Miklius, A., and Poland, M. (2008). *Evolution of Deformation Studies on Active Hawaiian Volcanoes.* Reston, VA: U.S. Geological Survey, 23. doi: 10.3133/sir20085090

Degrandpre, D., Wang, T., Lu, Z., and Freymueller, J. (2017). Episodic inflation and complex surface deformation of Akutan volcano, Alaska revealed from GPS time-series. *J. Volcanol. Geotherm. Res.* 347, 337–359. doi: 10.1016/j.jvolgeores.2017.10.003

Dietterich, H. R., Poland, M. P., Schmidt, D. A., Cashman, K. V., Sherrod, D. R., and Espinosa, A. T. (2012). Tracking lava flow emplacement on the East Rift Zone of Kīlauea, Hawai'i with synthetic aperture radar coherence. *Geochem. Geophys. Geosys. (G3)* 13:17. doi: 10.1029/2011GC004016

Dzurisin, D., Donnelly-Nolan, J. M., Evans, J. R., and Walter, S. R. (1991). Crustal subsidence, seismicity, and structure near Medicine Lake Volcano, California. *J. Geophys. Res.* 96, 16319–16333. doi: 10.1029/91JB01452

Dzurisin, D., Lisowski, M., and Wicks, C. W. (2009). Continuing inflation at three sisters volcanic center, central Oregon Cascade Range, USA, from GPS, leveling, and InSAR observations. *Bull. Volc.* 71, 1091–1110. doi: 10.1007/s00445-009-0296-4

Dzurisin, D., Lisowski, M., and Wicks, C. W. Jr. (2017). Semipermanent GPS (SPGPS) as a volcano monitoring tool: Rationale, method, and applications. *J. Volcanol. Geotherm. Res.* 34, 40–51. doi: 10.1016/j.jvolgeores.2017.03.007

Dzurisin. D., Lisowski, M., Wicks, C. W., Poland, M. P., and Endo, E. T. (2005). Geodetic observations and modeling of magmatic inflation at the Three Sisters volcanic center, central Oregon Cascade Range, USA. *J. Volcanol. Geotherm. Res.* 150, 1–3; The Changing Shape of Active Volcanoes, 35–54. doi: 10.1016/j.jvolgeores.2005.07.011

Dzurisin, D., Moran, S. C., Lisowski, M., Schilling, S. P., Anderson, K. R., and Werner, C. (2015). The 2004–2008 dome-building eruption at Mount St. Helens, Washington: epilogue. *Bull. Volc.* 77:89. doi: 10.1007/s00445-015-0973-4

Dzurisin, D., Poland, M. P., and Burgmann, R. (2002). Steady subsidence of Medicine Lake Volcano, Northern California, revealed by repeated levelling surveys. *J. Geophys. Res.* 107:B12. doi: 10.1029/2001JB000893

Dzurisin, D., Wicks, C. W, and Poland, M. P. (2012). *History of Surface Displacements at the Yellowstone Caldera, Wyoming, from Leveling Surveys and InSAR Observations, 1923–2008*. Reston, VA: U.S. Geological Survey, 68. Available at: http://pubs.usgs.gov/pp/1788/

Ebmeier, S. K., Biggs, J., Mather, T. A., and Amelung, F. (2013). On the lack of InSAR observations of magmatic deformation at Cetral American volcanoes. *J. Geophys. Res.* 118, 2571–2585. doi: 10.1002/jgrb.50195

Elliott, J. R., Walters, R. J., and Wright, T. J. (2016). The role of space-based observation in understanding and responding to active tectonics and earthquakes. *Nat. Commun.* 7:13844. doi: 10.1038/ncomms13844

Ewert, J. W. (2007). A system for ranking relative threats of U.S. *volcanoes*. *Nat. Hazards Rev.* 8, 112–124. doi: 10.1061/(ASCE)1527-6988(2007)8:4(112)

Ewert, J. W., Guffanti, M. C., and Murray, T. L. (2005). *An Assessment of Volcanic Threat and Monitoring Capabilities in the United States—Framework for a National Volcano Early Warning System*. Reston, VA: U.S. Geological Survey, 62. doi: 10.3133/ofr20051164

Ewert, J. W., Diefenbach, A. K., and Ramsey, D. W. (2018). *2018 Update to the U.S. Geological Survey National Volcanic Threat Assessment*. Reston, VA: U.S. Geological Survey, 40. doi: 10.3133/sir20185140

Foster, J., Kealy, J., Cherubini, T., Businger, S., Lu, Z., and Murphy, M. (2013). The utility of atmospheric analyses for the mitigation of artifacts in InSAR. *J. Geophys. Res.* 118, 748–758. doi: 10.1002/jgrb.50093

Fournier, R. O. (1999). Hydrothermal processes related to movement of fluid from plastic into brittle rock in the magmatic-epithermal environment. *Econ. Geol.* 94, 1193–1212. doi: 10.2113/gsecongeo.94.8.1193

Fournier, R. O. (2007). "Hydrothermal systems and volcano geochemistry," in *Volcano Deformation—Geodetic Monitoring Techniques*, Chap. 10, ed. D. Dzurisin (Berlin: Springer-Praxis Books), 323–341.

Gaddis, L., Mouginis-Mark, P. J., Singer, R. B., and Kaupp, V. (1989). Geologic analyses of Shuttle Imaging Radar (SIR-B) data of Kīlauea Volcano, Hawai'i. *Bull. Geol. Soc. Am.* 101, 317–332. doi: 10.1130/0016-7606(1989)101<0317:GAOSIR>2.3.CO;2

Hill, D. P. (1984). Monitoring unrest in a large silicic caldera, the Long Valley–Inyo Craters volcanic complex in east-central California. *Bull. Volcanol.* 47, 371–395. doi: 10.1007/BF01961568

Jo, M.-J., Jung, H.-S., Won, J.-S., and Lundgren, P. (2015). Measurement of three-dimensional surface deformation by Cosmo-SkyMed X-band radar interferometry: application to the March 2011 Kamoamoa fissure eruption, Kīlauea Volcano, Hawai'i. *Remote Sens. Environ.* 169, 176–191. doi: 10.1016/j.rse.2015.08.003

Kauahikaua, J. P. (2007). "Lava flow hazard assessment, as of August 2007, for Kīlauea East Rift Zone eruptions, Hawai'i Island," in *Proceedings of the U.S. Geological Survey Open-File Report 2007-1264*, Hawaii National Park, HI, 9.

Kauahikaua, J., Sherrod, D. R., Cashman, K. V., Heliker, C., Hon, K., Mattox, T. N., et al. (2003). Hawaiian lava-flow dynamics during the Pu'u 'Ō'ō-Kūpaianaha eruption: a tale of two decades. *U.S. Geol. Surv. Prof. Pap.* 1676, 63–88.

Langbein, J. (1989). Deformation of the long valley caldera, eastern California, from mid-1983 to mid-1988: measurements using a two-color geodimeter. *J. Geophys. Res.* 94, 3833–3850. doi: 10.1029/JB094iB04p03833

Langbein, J. O. (2003). Deformation of the Long Valley Caldera, California: inferences from measurements from 1988 to 2001. *J. Volcanol. Geotherm. Res.* 127, 247–267. doi: 10.1016/S0377-0273(03)00172-0

Liu, Z., Dong, D., and Lundgren, P. (2011). Constraints on time-dependent volcanic source models at Long Valley Caldera from 1996 to 2009 using InSAR and geodetic measurements. *Geophys. J. Int.* 187, 1283–1300. doi: 10.1111/j.1365-246X.2011.05214.x

Lowenstern, J. B., and Hurwitz, S. (2008). Monitoring a supervolcano in repose: heat and volatile flux at the Yellowstone Caldera. *Elements* 4, 35–40. doi: 10.2113/GSELEMENTS.4.1.35

Lu, Z. (1996). *Stress and Surface Deformation Due to Earthquakes and Volcanoes in Alaska*. Ph. D., dissertation, University of Alaska, Fairbanks, Alaska, 142.

Lu, Z., and Dzurisin, D. (2014). *InSAR Imaging of Aleutian Volcanoes—Monitoring a Volcanic Arc from Space*, 388. Berlin: Springer-Praxis Books, Geophysical Sciences. doi: 10.1007/978-3-642-00348-6

Lu, Z., and Dzurisin, D. (2018). "Radar monitoring of volcanic activities," in *Natural Hazards: Earthquakes, Volcanoes and Landslides*, eds R. Singh and D. Bartlett (Boca Raton, FL: CRC Press), 421–446. doi: 10.1201/9781315166841-18

Lu, Z., Fatland, R., Wyss, M., Li, S., Eichelberger, J., Dean, K., et al. (1997). Deformation of new trident volcano measured by ERS-1 SAR interferometry, Katmai National Park, Alaska. *Geophys. Res. Lett.* 24, 695–698. doi: 10.1029/97GL00539

Lu, Z., Masterlark, T., and Dzurisin, D. (2005a). Interferometric synthetic aperture radar (InSAR) study of Okmok volcano, Alaska, 1992-2003: magma supply dynamics and postemplacement lava flow deformation. *J. Geophys. Res.* 110:B02403. doi: 10.1029/2004JB003148

Lu, Z., Wicks, C., Kwoun, O., Power, J., and Dzurisin, D. (2005b). Surface deformation associated with the March 1996 earthquake swarm at Akutan Island, Alaska, revealed by C-band ERS and L-band JERS radar interferometry. *Can. J. Remote Sens.* 31, 7–20. doi: 10.5589/m04-054

Lu, Z., Mann, D., Freymueller, J., and Meyer, D. (2000a). Synthetic aperture radar interferometry of Okmok volcano, Alaska: radar observations. *J. Geophys. Res.* 105, 10791–10806. doi: 10.1029/2000JB900034

Lu, Z., Wicks, C., Power, J., and Dzurisin, D. (2000b). Ground deformation associated with the March 1996 earthquake swarm at Akutan volcano, Alaska, revealed by satellite radar interferometry. *J. Geophys. Res.* 105, 21483–21496. doi: 10.1029/2000JB900200

Lundgren, P., Poland, M., Miklius, A., Orr, T., Yun, S.-H., Fielding, E., et al. (2013). Evolution of dike opening during the March 2011 Kamoamoa fissure eruption, Kīlauea Volcano, Hawai'i. *J. Geophys. Res.* 118, 897–914. doi: 10.1002/jgrb.50108

Massonnet, D., Briole, P., and Arnaud, A. (1995). Deflation of Mount Etna monitored by spaceborne radar interferometry. *Nature* 375, 567–570. doi: 10.1038/375567a0

Massonnet, D., and Feigl, K. L. (1998). Radar interferometry and its application to changes in the Earth's surface. *Rev. Geophys.* 36, 441–500. doi: 10.1029/97RG03139

Massonnet, D., Rossi, M., Carmona, C., Adragna, F., Peltzer, G., Feigl, K., et al. (1993). The displacement field of the Landers earthquake mapped by radar interferometry. *Nature* 364, 138–142.

Meertens, C. M., Smith, R. B., and Puskas, C. M. (2000). Crustal deformation of the Yellowstone caldera from campaign and continuous GPS surveys, 1987–2000. *EOS Trans. Am. Geophys. Union* 81, V22F–19.

Meyer, F. J., McAlpin, D. B., Gong, W., Ajadi, O., Arko, S., Webley, P. W., et al. (2015). Integrating SAR and derived products into operational volcano monitoring and decision support systems. *ISPRS J. Photogramm. Remote Sens.* 100, 106–117. doi: 10.1016/j.isprsjprs.2014.05.009

Miller, T. P., and Smith, R. L. (1987). Late quaternary caldera-forming eruptions in the Eastern Aleutian arc, Alaska. *Geology* 15, 434–438. doi: 10.1130/0091-7613(1987)15<434:LQCEIT>2.0.CO;2

Montgomery-Brown, E. K., Sinnett, D. K., Larson, K. M., Poland, M. P., Segall, P., and Miklius, A. (2011). Spatiotemporal evolution of dike opening and décollement slip at Kīlauea Volcano, Hawai'i. *J. Geophys. Res.* 116:B03401. doi: 10.1029/2010JB007762

Montgomery-Brown, E. K., Sinnett, D. K., Poland, M., Segall, P., Orr, T., Zebker, H., et al. (2010). Geodetic evidence for en echelon dike emplacement and concurrent slow-slip during the June 2007 intrusion and eruption at Kīlauea volcano, Hawai'i. *J. Geophys. Res.* 115:15. doi: 10.1029/2009JB006658

Montgomery-Brown, E. K., Wicks, C. W., Cervelli, P. F., Langbein, J. O., Svarc, J. L., Shelly, D. R., et al. (2015). Renewed inflation of long Valley Caldera, California (2011–2014). *Geophys. Res. Lett.* 42, 5250–5257. doi: 10.1002/2015GL064338

Murray, J. R., and Svarc, J. (2017). Global positioning system data collection, processing, and analysis conducted by the U.S. Geological Survey Earthquake Hazards Program. *Seismol. Res. Lett.* 88, 916–925. doi: 10.1785/0220160204

Myrhaug, D., and Rue, H. (1998). Joint distribution of successive wave periods revisited. *J. Ship Res.* 42, 199–206.

Nikkhoo, M., and Walter, T. R. (2015). Triangular dislocation: an analytical, artefact-free solution. *Geophys. J. Int.* 201, 1119–1141, doi: 10.1093/gji/ggv035

Nikkhoo, M., Walter, T. R., Lundgren, P. R., and Prats-Iraola, P. (2017). Compound dislocation models (CDMs) for volcano deformation analyses. *Geophys. J. Int.* 208, 877–894. doi: 10.1093/gji/ggw427

Okada, Y. (1985). Surface deformation due to shear and tensile faults in a half-space. *Bull. Seis. Soc. Am.* 75, 1135–1154.

Parker, A. L., Biggs, J., and Lu, Z. (2014). Investigating long-term subsidence at Medicine Lake Volcano, CA, using multitemporal InSAR. *Geophys. J. Int.* 199, 844–859. doi: 10.1093/gji/ggu304

Parker, A. L., Biggs, J., and Lu, Z. (2016). Time-scale and mechanism of subsidence at Lassen Volcanic Center, CA, from InSAR. *J. Volcanol. Geotherm. Res.* 320, 117–127. doi: 10.1016/j.jvolgeores.2016.04.013

Patrick, M. R., Kauahikaua, J., Orr, T., Davies, A., and Ramsey, M. (2015). Operational thermal remote sensing and lava flow monitoring at the Hawaiian Volcano Observatory. *Geol. Soc. London Spec. Publ.* 426, 489–503. doi: 10.1144/sp426.17

Poland, M., Bawden, G., Lisowski, M., and Dzurisin, D. (2004). Newly discovered subsidence at Lassen Peak, southern Cascade Range, California, from InSAR and GPS. *EOS Trans. Am. Geophys. Union Fall Meet. Suppl.* 85:G51 A-0068.

Poland, M. P., Burgmann, R., Dzurisin, D., Lisowski, M., Masterlark, T., Owen, S., et al. (2006). Constraints on the mechanism of long-term, steady subsidence at Medicine Lake Volcano, northern California, from GPS, levelling and InSAR. *J. Volc. Geotherm. Res.* 150, 55–78. doi: 10.1016/j.jvolgeores.2005.07.007

Poland, M. P. (2010). Localized surface disruptions observed by InSAR during strong earthquakes in Java and Hawai'i. *Bull. Seismol. Soc. Am.* 100, 532–540. doi: 10.1785/0120090175

Poland, M. P. (2014). Time-averaged discharge rate of subaerial lava at Kīlauea Volcano, Hawai'i, measured from TanDEM-X interferometry: implications for magma supply and storage during 2011–2013. *J. Geophys. Res.* 119, 5464–5481. doi: 10.1002/2014JB011132

Poland, M. P., Lisowski, M., Dzurisin, D., Kramer, R., McLay, M., and Pauk, B. (2017). Volcano geodesy in the Cascade arc, USA. *Bull. Volcanol.* 79:33. doi: 10.1007/s00445-017-1140-x

Poland, M. P., and Lu, Z. (2008). "Radar interferometry observations of surface displacements during pre- and coeruptive periods at Mount St. Helens, Washington, 1992–2005. U.S. Geological Survey Professional Paper 1750", in *A Volcano Rekindled: The Renewed Eruption of Mount St. Helens, 2004-2006*, eds D. R. Sherrod, W. E. Scott, and P. H. Stauffer (Reston, VA: U.S. Geological Survey), 361–386.

Pritchard, M. E., and Simons, M. (2004a). An InSAR-based survey of volcanic deformation in the central Andes. *Geochem. Geophys. Geosys.* 5:42. doi: 10.1029/2003GC000610

Pritchard, M. E., and Simons, M. (2004b). Surveying volcanic arcs with satellite radar interferometry: the central Andes, Kamchatka, and beyond. *GSA Today* 14, 4–10. doi: 10.1130/1052-51732004014<4:SVAWSR<2.0.CO;2

Pritchard, M. E., and Yun, S.-H. (2018). "Satellite radar imaging and its application to natural hazards," in *Natural Hazards: Earthquakes, Volcanoes and Landslides*, eds R. S. Singh and D. Bartlett (Boca Raton, FL: CRC Press), 95–114. doi: 10.1201/9781315166841-5

Richter, N., Poland, M. P., and Lundgren, P. R. (2013). TerraSAR-X interferometry reveals small-scale deformation associated with the summit eruption of Kīlauea Volcano, Hawai'i. *Geophys. Res. Lett.* 40, 1279–1283. doi: 10.1002/grl.50286

Riddick, S. N., and Schmidt, D. A. (2011). Time-dependent changes in volcanic inflation rate near Three Sisters, Oregon, revealed by InSAR. *Geochem. Geophys. Geosyst.* 12:Q12005. doi: 10.1029/2011GC003826

Poland, M. P., and Orr, T. R. (2014). Identifying hazards associated with lava deltas. *Bull. Volc.* 76:12. doi: 10.1007/s00445-014-0880-0

Poland, M. P., Miklius, A., and Montgomery-Brown, E. K. (2014). "Magma supply, storage, and transport at shield-stage Hawaiian volcanoes," in *Characteristics of Hawaiian Volcanoes*, Chap. 5, eds M. P. Poland, T. J. Takahashi, and C. M. Landowski (Reston, VA: U.S. Geological Survey), 179–234. doi: 10.3133/pp18015

Poland, M. P., Orr, T. R., Kauahikaua, J. P., Brantley, S. R., Babb, J. L., and Patrick, M. R. (2016). The 2014–2015 Pāhoa lava flow crisis at Kīlauea Volcano, Hawai'i: disaster avoided and lessons learned. *GSA Today* 26, 4–10. doi: 10.1130/GSATG262A.1

Rosen, P. A., Hensley, S., Zebker, H. A., Webb, F. H., and Fielding, E. J. (1996). Surface deformation and coherence measurements of Kīlauea Volcano, Hawai'i, from SIR-C radar interferometry. *J. Geophys. Res.* 101, 23109–23125. doi: 10.1029/96JE01459

Salvi, S., Poland, M. P., Sigmundsson, F., Puglisi, G., Borgstrom, S., Ergintav, S., et al. (2017). "From open data to science-based services for disaster risk management," in *Proceedings of the Experience of the GEO Geohazards Supersite Network: EOS Fall Meeting*, AGU, New Orleans, Louis.

Savage, J. C. (1988). Principal component analysis of geodetically measured deformation in the Long Valley caldera, eastern California, 1983–1987. *J. Geophys. Res.* 93, 13297–13306. doi: 10.1029/JB093iB11p13297

Savage, J. C., and Clark, M. M. (1982). Magmatic resurgence in long Valley caldera, California: possible cause of the 1980 Mammoth Lakes earthquakes. *Science* 217, 531–533. doi: 10.1126/science.217.4559.531

Scott, W. E., Iverson, R. M., Schilling, S. P., and Fischer, B. J. (2001). *Volcano Hazards in the Three Sisters Region, Oregon*. Reston, VA: U.S. Geological Survey, 14. doi: 10.3133/ofr99437

Segall, P. (2010). *Earthquake and Volcano Deformation*. Princeton, NJ: Princeton University Press, 432. doi: 10.1515/9781400833856

Sherrod, D. R., Taylor, E. M., Ferns, M. L., Scott, W. E., Conrey, R. M., and Smith, G. A. (2004). *Geologic Map of the Bend 30- by 60-minute Quadrangle, Central Oregon*. Reston, VA: U.S. Geological Survey.

Swanson, D. A., Fiske, R. S., Thornber, C. T., and Poland, M. P. (2018). *Dikes in the Koa'e Fault System, and the Koa'e-east Rift Zone Structural Grain*. Volcano, HI: Geological Society of America.

Thatcher, W., and Massonnet, D. (1997). Crustal deformation at Long Valley Caldera, eastern California, 1992–1996 inferred from satellite radar interferometry. *Geophys. Res. Lett.* 24, 2519–2522. doi: 10.1029/97GL02597

Tizzani, P., Battaglia, M., Zeni, G., Atzori, S., Berardino, P., and Lanari, R. (2009). Uplift and magma intrusion at Long Valley caldera from InSAR and gravity measurements. *Geology* 37, 63–66. doi: 10.1130/G25318A.1

Waite, G. P., and Smith, R. B. (2002). Seismic evidence for fluid migration accompanying subsidence of the Yellowstone caldera. *J. Geophys. Res.* 107:15. doi: 10.1029/2001JB000586

Wang, T., Degrandpre, D., Lu, Z., and Freymueller, J. (2018). Complex surface deformation of Akutan volcano, Alaska revealed from InSAR time series. *Int. J. Appl. Earth Observ. Geoinform.* 64, 171–180. doi: 10.1016/j.jag.2017.09.001

Wang, T., Poland, M. P., and Lu, Z. (2015). Dome growth at mount cleveland, Aleutian Arc, quantified by time series TerraSAR-X imagery. *Geophys. Res. Lett.* 42, 10614–10621. doi: 10.1002/2015GL066784

Werner, C., and Brantley, S. (2003). CO2 emissions from the Yellowstone volcanic system. *Geochem. Geophys. Geosyst.* 4:1061. doi: 10.1029/2002GC000473

Wicks, C. Jr., Thatcher, W., and Dzurisin, D. (1998). Migration of fluids beneath Yellowstone Caldera inferred from satellite radar interferometry. *Science* 282, 458–462. doi: 10.1126/science.282.5388.458

Wicks, C. W. Jr., Dzurisin, D., Ingebritsen, S., Thatcher, W., Lu, Z., and Iverson, J. (2002). Magmatic activity beneath the quiescent Three Sisters volcanic center, central Oregon Cascade Range, USA. *Geophys. Res. Lett.* 29:7. doi: 10.1029/2001GL014205

Wicks, C. W., Thatcher, W., Dzurisin, D., and Svarc, J. (2006). Uplift, thermal unrest, and magma intrusion at Yellowstone Caldera, observed with InSAR. *Nature* 440, 72–75. doi: 10.1038/nature04507

Zebker, H. A., Rosen, P., Hensley, S., and Mouginis-Mark, P. J. (1996). Analysis of active lava flows on Kilauea Volcano, Hawaii, using SIR-C radar correlation measurements. *Geology* 24, 495–498.

Conflict of Interest Statement: The authors declare that the research was conducted in the absence of any commercial or financial relationships that could be construed as a potential conflict of interest.

Copyright © 2019 Dzurisin, Lu, Poland and Wicks. This is an open-access article distributed under the terms of the Creative Commons Attribution License (CC BY). The use, distribution or reproduction in other forums is permitted, provided the original author(s) and the copyright owner(s) are credited and that the original publication in this journal is cited, in accordance with accepted academic practice. No use, distribution or reproduction is permitted which does not comply with these terms.